IEICE TRANS. ELECTRON., VOL.E107–C, NO.4 APRIL 2024

PAPER *Special Section on Recent Progress in Electromagnetic Theory and Its Application*

Coupling Analysis of Fiber-Type Polarization Splitter

Taiki ARAKAWA[†], **Kazuhiro YAMAGUCHI**[†], **Kazunori KAMEDA**[††], ***and*** **Shinichi FURUKAWA**[†a)], ***Members***

SUMMARY We study the device length and/or band characteristics examined by two coupling analysis methods for our proposed fiber-type polarization splitter (FPS) composed of single mode fiber and polarization maintaining fiber. The first method is based on the power transition characteristics of the coupled-mode theory (CMT), and the second, a more accurate analysis method, is based on improved fundamental mode excitation (IFME). The CMT and IFME were evaluated and investigated with respect to the device length and bandwidth characteristics of the FPS. In addition, the influence of the excitation point shift of the fundamental mode, which has not been almost researched so far, is also analysed by using IFME.

key words: *polarization splitter, device length, band characteristics, coupling analysis, excitation problem*

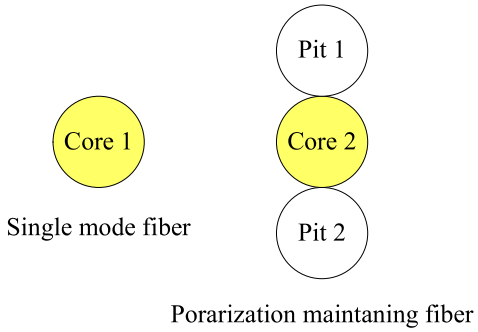

Fig. 1 Cross section of FPS analyzed coupling characteristics.

1. Introduction

Polarization splitters are fiber-type devices that actively utilise the coupling characteristics of optical fibers [1]–[10]. Such fiber polarization splitters (FPSs) are required to split the fundamental mode (HE_{11} mode) of a single-mode fiber into two orthogonal polarizations (HE_{11}^{x} mode: x-polarization and HE_{11}^{y} mode: y-polarization). Therefore, a combined of structure of single-mode fiber (SMF) and polarization maintaining fiber (PMF) is generally adopted [4], [7]–[9]. The accuracy of the coupling analysis between the SMF and PMF is important in designing FPSs. In many coupling problems, coupled-mode theory (CMT) [11]–[15] is used for analysis. Notably, CMT is applicable only when weak coupling is present. In our previous studies [16]–[18], under weak coupling, the device length and bandwidth of the FPS were calculated using the CMT, and the propagation constants were obtained using the multipole method. Previously, we proposed fundamental mode excitation (FME)-based analysis combined with point matching method (PMM) to obtain more rigorous coupling characteristics even under strong coupling [19], [20], and the results for the FPS design were reported [9], [10], [21]. The FME can be used to analyse the propagation status of the Poynting vector in addition to the power transition characteristics and is also applicable to the case of strong coupling. However, because this FME is not supported by an arbitrary arrangement of circular cores and pits, inhomogeneous circular cores, and excitation from arbitrary positions in the cross-sections of the coupling system, we recently developed an improved FME (IFME) [22] to address the aforementioned issues. To date, the IFME has only been used as part of the characterisation of optical directional couplers [22], [23] and has not been applied to the design of FPS.

In this study, we investigated the power transition characteristics, device length, and band characteristics of IFME and CMT for FPS (Fig. 1) composed of an SMF with a single core and a PMF with circular pits in contact with the upper and lower sides of the single core. We also investigated the influence of band characteristics when the fundamental mode exciting the SMF deviates from the core center using IFME, which cannot be calculated by CMT.

2. Formulation

The formulation methods are described by separating them into the analysis of the propagation constants (Sect 2.1) and coupling analysis by IFME (Sect. 2.2).

2.1 Analysis of Propagation Constants

As an analysis method of propagation constants, PMM-DM [24]–[27] combines the point-matching method (PMM) and the difference method (DM). The PMM is suitable for high-precision analysis of FPS with arbitrarily arranged circular regions, and the DM is suitable for the analysis of cores with axially symmetrical arbitrary refractive index profiles. The formulation of the PMM-DM only describes the main points of the analysis. The cross-section and coordinate system used for the analysis are shown in Fig. 2. The center of an arbitrarily arranged circular area is defined as origin O_i

Manuscript received April 10, 2023.
Manuscript revised July 26, 2023.
Manuscript publicized October 27, 2023.

[†]The authors are with Nihon University, Tokyo, 101–8308 Japan.
[††]The author is with Sano Nihon University College, Sano-shi, 327–0821 Japan.
a) E-mail: furukawa.shinichi@nihon-u.ac.jp

DOI: 10.1587/transele.2023REP0003

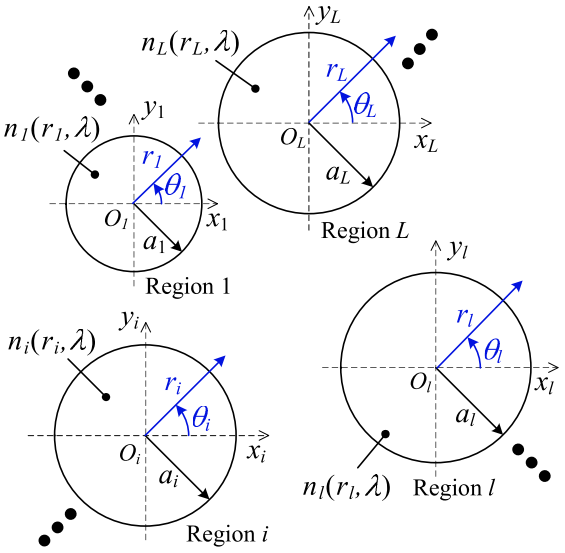

Fig. 2 Cross section and coordinate system.

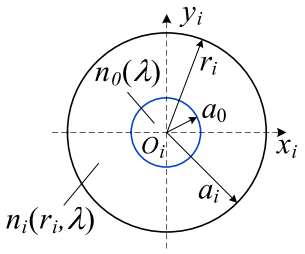

Fig. 3 Cross section of core region.

($i = 1, 2, 3, \cdots, L$). The electromagnetic field in each circular region is expanded using a cylindrical coordinate system. Assuming that the z-axis is perpendicular to the plane of the paper, the wave is propagated along the z-axis in proportion to the factor $\exp(j\omega t - j\beta z)$ (ω: angular frequency, β: propagation constant). In this study, the circular regions comprised cores and pits. The refractive index of the core or pit region (the region of radius a_i centerd on origin O_i) has an inhomogeneous refractive index $n(r_i, \lambda)$ (λ: wavelength in vacuum) in the radial direction, and the refractive index of the external region (clad region) is $n_c(\lambda)$. The electromagnetic fields in each region of the PMM-DM used to analyse the propagation constants are as follows:

Core region:

The cross section of the core region is shown in Fig. 3. Considering the boundary condition at the center O_i, the formulation is divided into the vicinity of the center O_i (core region I with $n_0(\lambda)$ in the range of $0 \le r_i \le a_0$) and other regions (core region II with $n(r_i, \lambda)$ in the range of $a_0 \le r_i \le a_i$) [28].

- Core region I

$$E_{zi} = \sum_{m=-\infty}^{\infty} A_m^{0(i)} J_m(\eta r_i) \exp(-jm\theta_i) \tag{1}$$

$$H_{zi} = \sum_{m=-\infty}^{\infty} B_m^{0(i)} J_m(\eta r_i) \exp(-jm\theta_i) \tag{2}$$

- Core region II

$$E_{zi} = \sum_{m=-\infty}^{\infty} A_m^{(i)} E_{zm}(r_i) \exp(-jm\theta_i) \tag{3}$$

$$H_{zi} = \sum_{m=-\infty}^{\infty} B_m^{(i)} H_{zm}(r_i) \exp(-jm\theta_i) \tag{4}$$

$$E_{\theta i} = \sum_{m=-\infty}^{\infty} C_m^{(i)} E_{\theta m}(r_i) \exp(-jm\theta_i) \tag{5}$$

$$H_{\theta i} = \sum_{m=-\infty}^{\infty} D_m^{(i)} H_{\theta m}(r_i) \exp(-jm\theta_i) \tag{6}$$

The electromagnetic fields, $E_{zm}(r_i)$, $H_{zm}(r_i)$, $E_{\theta m}(r_i)$, and $H_{\theta\nu}(r_i)$ in core region II are obtained by solving the simultaneous ordinary differential Eqs. (7)–(10) in the range of $a_0 \le r_i \le a_i$.

$$\frac{dE_{zm}(r_i)}{dr_i} = j\frac{m}{r_i}\frac{\beta}{kn(r_i,,\lambda)^2}H_{zm}(r_i) + jk\left\{1 - \left(\frac{\beta}{kn(r_i,\lambda)}\right)^2\right\}H_{\theta m}(r_i), \tag{7}$$

$$\frac{dH_{zm}(r_i)}{dr_i} = -j\frac{m}{r_i}\frac{\beta}{kn(r_i,\lambda)^2}E_{zm}(r_i) - jk\left\{n(r_i,\lambda)^2 - \left(\frac{\beta}{k}\right)^2\right\}E_{\theta m}(r_i), \tag{8}$$

$$\frac{dE_{\theta m}(r_i)}{dr_i} = -jk\left\{1 - \left(\frac{m}{r_i}\right)^2\frac{1}{(kn(r_i,\lambda))^2}\right\}H_{zm}(r_i) - j\frac{1}{r_i}E_{\theta m}(r_i) - j\frac{m}{r_i}\frac{\beta}{kn(r_i,\lambda)^2}H_{\theta m}(r_i), \tag{9}$$

$$\frac{dH_{\theta m}(r_i)}{dr_i} = j\frac{1}{k}\left\{(kn(r_i,\lambda))^2 - \left(\frac{m}{r_i}\right)^2\right\}E_{zm}(r_i) + j\frac{m}{r_i}\frac{\beta}{k}E_{\theta m}(r_i) - j\frac{1}{r_i}H_{\theta m}(r_i), \tag{10}$$

where $A_m^{(i)}$ and $B_m^{(i)}$ are the coefficients of electromagnetic fields, $\eta_i^2 \triangleq n_i^2(\lambda)k^2 - \beta^2$; k is the wave number in vacuum; and $J_m()$ is the Bessel function of the first kind. For $n_0(\lambda)k < \beta$ in Eqs. (1) and (2) (core region I), $J_m()$ and η are replaced with $I_m()$ and ξ ($\xi^2 \triangleq \beta^2 - n_0^2(\lambda)k^2$), respectively. $I_m()$ is a modified Bessel function of the first type. Equations (7)–(10) can be solved using the numerical solutions of ordinary differential equations.

Pit regions [$n_i(\lambda) = 1.0$]:

$$E_{zi} = \sum_{m=-\infty}^{\infty} F_m^{(i)} I_m(\xi_i r_i) \exp(-jm\theta_i), \tag{11}$$

$$H_{zi} = \sum_{m=-\infty}^{\infty} G_m^{(i)} I_m(\xi_i r_i) \exp(-jm\theta_i), \tag{12}$$

where $F_m^{(i)}$ and $G_m^{(i)}$ are the coefficients of electromagnetic

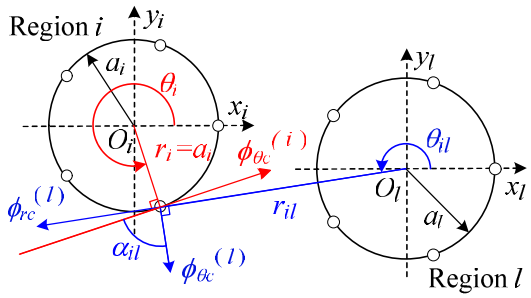

Fig. 4 Boundary condition at each point by PMM.

fields, $\xi_i^2 \triangleq \beta^2 - n_i^2(\lambda)k^2$.

The Cladding region is given by:

$$E_{zc} = \sum_{i=1}^{L}\sum_{m=-\infty}^{\infty} Q_m^{(i)} K_m(\xi_c r_i)\exp(-jm\theta_i), \tag{13}$$

$$H_{zc} = \sum_{i=1}^{L}\sum_{m=-\infty}^{\infty} R_m^{(i)} K_m(\xi_c r_i)\exp(-jm\theta_i), \tag{14}$$

where $Q_m^{(i)}$ and $R_m^{(i)}$ are the coefficients of electromagnetic fields, $\xi_c^2 \triangleq \beta^2 - n_c^2(\lambda)k^2$, and $K_m()$ is the modified Bessel function of the second kind. In the numerical calculation, $\sum_{m=-\infty}^{\infty}$ [in Eqs. (1)–(6) and Eqs. (11)–(14)] is approximated using $\sum_{m=-N}^{N}$ with a finite number, N, of modes. We applied PMM to the boundaries of each region. The propagation constants required for the analysis of coupling characteristics can be computed using the eigenvalue equations obtained by imposing the following simple boundary conditions at each point (Fig. 4):

$$\begin{aligned}\phi_{zi}(r_i,\theta_i) &= \phi_{zc}^{(i)}(r_i,\theta_i) \\ &\quad + \sum_{l=1}^{L}(1-\delta_{il})\phi_{zc}^{(l)}(r_{il},\theta_{il}),\end{aligned} \tag{15}$$

$$\begin{aligned}\phi_{\theta i}(r_i,\theta_i) &= \phi_{\theta c}^{(i)}(r_i,\theta_i) \\ &\quad + \sum_{l=1}^{L}(1-\delta_{il})\{\phi_{\theta c}^{(l)}(r_{il},\theta_{il})\cos(\alpha_{il}) \\ &\quad + \phi_{rc}^{(l)}\sin(\alpha_{il})\},\end{aligned} \tag{16}$$

where $\phi \triangleq E$ or H and δ_{il} is Kronecker delta. The r and θ-components of the electromagnetic fields synthesised at the boundary were derived from Maxwell's equations.

2.2 Coupling Analysis by IFME

Because the coupling analysis of the CMT is performed by substituting only the propagation constant into the coupled-mode equation, it does not depend on the analysis method of the propagation constants. However, in the coupling analysis of the IFME, the electromagnetic fields propagating in the coupled system depend on the analytical method of the propagation constants. Therefore, IFME must be used in combination with PMM-DM.

In IFME, the transverse components of the electromagnetic fields $\boldsymbol{E}_t^{(\gamma)}$ and $\boldsymbol{H}_t^{(\gamma)}$ ($\gamma = x, y$) in the coupling system can be classified into the following two polarizations.

x-polarization:

$$\boldsymbol{E}_t^{(x)} = \sum_{m=1}^{M_x} C_m^{(x)} \boldsymbol{e}_{mt}^{(x)} f_m^{(x)}, \tag{17}$$

$$\boldsymbol{H}_t^{(x)} = \sum_{m=1}^{M_x} C_m^{(x)} \boldsymbol{h}_{mt}^{(x)} f_m^{(x)}, \tag{18}$$

where M_x is the mode number of x-polarization. $C_m^{(x)}$ is the coefficient determined from the excitation condition, $\boldsymbol{e}_{mt}^{(x)}$ and $\boldsymbol{h}_{mt}^{(x)}$ are the transverse components of x-polarization electromagnetic field, $f_m^{(x)} \triangleq \exp(j\omega t - j\beta_m^{(x)} z)$, $\beta_m^{(x)}$: the propagation constant of x-polarization.

y-polarization:

$$\boldsymbol{E}_t^{(y)} = \sum_{m=1}^{M_y} C_m^{(y)} \boldsymbol{e}_{mt}^{(y)} f_m^{(y)}, \tag{19}$$

$$\boldsymbol{H}_t^{(y)} = \sum_{m=1}^{M_y} C_m^{(y)} \boldsymbol{h}_{mt}^{(y)} f_m^{(y)}, \tag{20}$$

where M_y is the mode number of y-polarization. $C_m^{(y)}$ is the coefficient determined from the excitation condition, $\boldsymbol{e}_{mt}^{(y)}$ and $\boldsymbol{h}_{mt}^{(y)}$ are the transverse components of y-polarization electromagnetic field, $f_m^{(y)} \triangleq \exp(j\omega t - j\beta_m^{(y)} z)$, and $\beta_m^{(y)}$: the propagation constant of y-polarization.

The electromagnetic field exciting Core 1 at $z = 0$ is assumed to be the HE_{11} mode (x- and y-polarizations) for a fiber with a single core. $C_m^{(x)}$ is determined by matching the transverse component of the x-polarizations in the splitter with that of the x-polarizations in a single-core fiber on the splitter cross section ($z = 0$). $C_m^{(y)}$ is determined by matching the transverse component of the y-polarization in the splitter and that of the y-polarizations in a single-core fiber on the cross section of the splitter ($z = 0$).

To obtain the coupling characteristics (power transition characteristics), the normalised power $P_1^{(\gamma)}$ inside Core 1 and the same quantity $P_2^{(\gamma)}$ inside Core 2 are defined as follows: When the Poynting vector of each polarization propagating in the splitter is $\bar{S}^{(\gamma)}(x,y,z)$ ($\gamma = x$ or y),

$$P_i^{(\gamma)}(z) = \frac{\displaystyle\int_{A_i} \bar{S}^{(\gamma)}(x,y,z)dxdy}{\displaystyle\int_{-\infty}^{\infty}\int_{-\infty}^{\infty} \bar{S}^{(\gamma)}(x,y,z)dxdy}, \tag{21}$$

where $\bar{S}^{(\gamma)}(x,y,z) = (1/2)Re\{[\boldsymbol{E}_t^{(\gamma)} \times \boldsymbol{H}_t^{(\gamma)*}]_z\}$, Re{ } is the real part of { }, [ ]$_z$ is the z component of [ ], $\boldsymbol{H}_t^{(\gamma)*}$ is the complex conjugate of $\boldsymbol{H}_t^{(\gamma)}$, and A_i is the area of the cross-section of core i.

In FPS with structure shown in Fig. 1, the HE_{11} mode

is split into two x-polarization [with the propagation constants [$\beta_1^{(x)}$, $\beta_2^{(x)}$ ($\beta_1^{(x)} > \beta_2^{(x)}$)] and two y-polarization [with the propagation constants [$\beta_1^{(y)}$, $\beta_2^{(y)}$ ($\beta_1^{(y)} > \beta_2^{(y)}$)]. Thus, the coupling analysis is discussed for cases where only four polarization modes ($\beta_1^{(x)}$, $\beta_2^{(x)}$, $\beta_1^{(y)}$, $\beta_2^{(y)}$) propagate, and M_x in Eqs. (17) and (18) and M_y in Eqs. (19) and (20) are set to $M_x = 2$ and $M_y = 2$, respectively.

3. Numerical Analysis

The FPS-analysed coupling characteristics are designed to output x-polarization from SMF and y-polarization from PMF at $z = L_y$ (L_y: device length) after excitation of the fundamental mode to fiber 1 at $z = 0$ (Fig. 5). The cross-sectional and structural parameters of the FPS and refractive index profiles in the cores of the SMF and PMF are shown in Fig. 6. The refractive-index profiles in the core of the SMF are step- or graded-type, whereas those of the PMF are step-type. The refractive index of each region is expressed

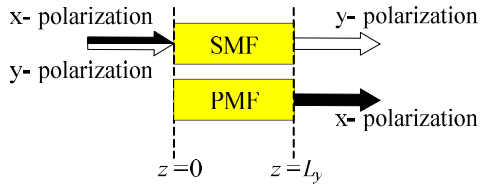

Fig. 5 Relationship between a behavior of the polarization splitter and the device length.

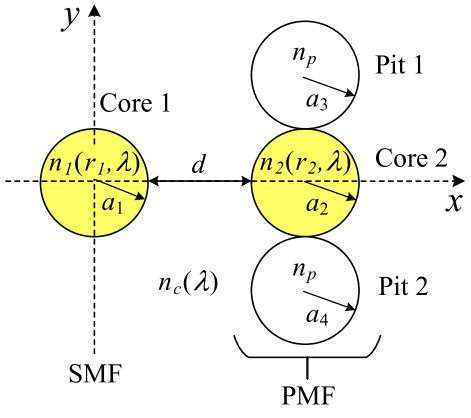

(a) Cross section and structural parameters of FPS.

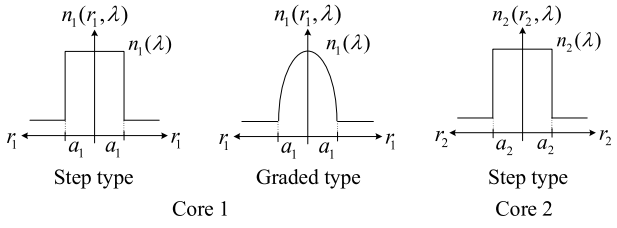

(b) Refractive index profile of Core 1 and Core 2.

Fig. 6 Structure of the analyzed FPS.

by the following equations [29].
Core 1 (SMF):

$$n_1(r_1, \lambda) = [n_G(\lambda) - n_S(\lambda)]\{d(r_1)/d^G\} + n_S(\lambda) \quad (22)$$

- Step type: $d(r_1) = d_1^G$
- Graded type: $d(r_1) = d_1^G\{1 - (r_1/a_1)^2\}$

Core2 (PMF):

$$n_2(r_2, \lambda) = [n_G(\lambda) - n_S(\lambda)]\{d_2^G/d^G\} + n_S(\lambda) \quad (23)$$

The outer cladding (common cladding of SMF and PMF):

$$n_C(\lambda) = n_S(\lambda) \quad (24)$$

Pits 1 and 2 (pits in PMF):

$$n_p = 1.0 \quad (25)$$

where $n_S(\lambda)$ is the refractive index of pure silica; $n_G(\lambda)$ is the refractive index of germanium-doped silica with a 5.8 mol% doping level of germanium ($d^G = 5.8$, d^G: reference doping level); d_i^G ($i = 1, 2$) is the doping level of germanium; The spectral dependence of $n_S(\lambda)$, $n_G(\lambda)$, and $n_F(\lambda)$ is considered using three-term Sellmeier equations [30]. The relative index difference of cores 1 and 2 and the inner cladding for the outer cladding is defined by

$$\Delta_i(\lambda) \triangleq [n_i(\lambda) - n_C(\lambda)]/n_C(\lambda), \quad (26)$$

where $i = 1$ (Core 1) or 2 (Core 2). The relative index difference, $\Delta_i(\lambda)$ at $\lambda = 1550$ nm is denoted as Δ_i in the figures and results. The width between Cores 1 and 2 is d, and the two pits (Pit 1 and Pit 2 in the PMF) contact the top and bottom of Core 2, respectively. Core radii a_1 (Core 1), a_2 (Core 2), a_3 (Pit 1), and a_4 (Pit 2) are assumed to have the same values ($a_1 = a_2 = a_3 = a_4$). In the following numerical analyses, the operation wavelengths, λ_{op}, is set to $\lambda_{op} = 1550$ nm and the relative index differences Δ_2 (Core 2) are set to $\Delta_2 = 1.0\%$.

3.1 Accuracy

The accuracy of the propagation constant, which is important in the coupling analyses (IFME and CMT) of the FPS, is determined by the number of modes (N) of the PMM and the number of steps (M) of the analysis method adopted as the DM. We considered the 4$^{\text{th}}$-order Runge-Kutta method as DM. The relationship between N, M, and significant digits for the propagation constant of step type and graded type (see profile of Fig. 6 (b)) is shown in Fig. 7 (the operation wavelength: $\lambda_{op} = 1550$ nm; step type: $\Delta_1 = 0.5514\%$, $\Delta_2 = 1.0\%$, $a_1 = 2.043$ μm, and $d/a_1 = 3.230$ [16]; graded type: $\Delta_1 = 0.9577\%$, $\Delta_2 = 1.0\%$, $a_1 = a_1 = 2.043$ μm, and $d/a_1 = 3.180$ [18]). Significant digits were calculated as follows:

$$\text{Significant digits} = -log_{10}|(S_t - S)/S|, \quad (27)$$

where S_t is the true value obtained by extrapolating from

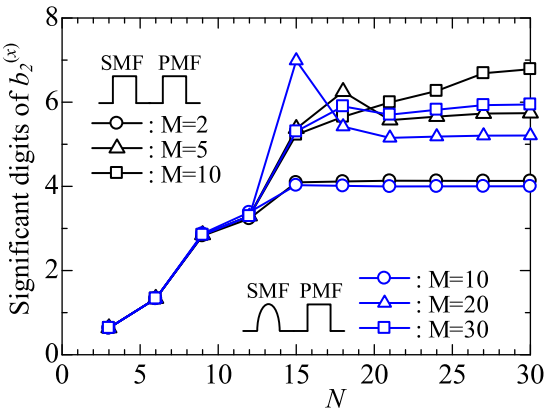

Fig. 7 Significant digits of propagation constants $b_2^{(x)} \triangleq \left[(b_2^{(x)}/k)^2 - n_c^2(\lambda_{op})\right] / \left[n_2^2(\lambda_{op}) - n_c^2(\lambda_{op})\right]$ *versus* mode number N of the point matching method.

S. In Fig. 7, only the result of the normalized propagation constant $b_2^{(x)}$, which is the least accurate among the four propagation constants used for analysis, is shown. As shown, the values of $b_2^{(x)}$ for the step type and $b_2^{(x)}$ for the graded type can be maintained at a precision of ≥ 4 digits by setting $N \geq 15$ and $M \geq 2$ and $N \geq 15$ and $M \geq 20$, respectively. In the case of SMF, the reason why $b_2^{(x)}$ converges in ≥ 4 at $M \geq 2$ is from analyzing with $a_0 = h$ ($\triangleq 1/N$, step size,). In the coupling analysis of the FPS (Sect. 3.2), the four propagation constants are calculated using N and M values such that an accuracy of ≥ 4 digits is maintained.

3.2 Coupling Analysis of FPS

In coupling analysis, the value of the core radius a (step type: $a_1 = 2.043$ μm, graded type: $a_1 = 2.043$ μm) and the value of the relative index difference Δ_1 (step type: $\Delta_1 = 0.5514\%$, graded type: $\Delta_1 = 0.9577\%$) were obtained according to the design procedure [16], [18] of the FPS with the structure shown in Fig. 6. The device length L_y was designed while changing the normalised core spacing d/a_1. The CMT was designed such that $l_x = 2l_y$ (l_x: coupling length of x-polarization, l_y: coupling length of y-polarization), and the IFME was designed such that the first z at which $P_1^{(y)}(z)$ is maximised coincides with the z at which $P_1^{(x)}(z)$ is first minimised. Using the designed structural parameters and the device length, the bandwidth was calculated from $P_1^{(\gamma)}(z)$ and $P_2^{(\gamma)}(z)$ ($\gamma = x$ or y) of the coupled-mode equation in CMT [16], and from $P_1^{(\gamma)}(z)$ and $P_2^{(\gamma)}(z)$ ($\gamma = x$ or y) of Eq. (9) in IFME.

In IFME, electromagnetic fields in the fundamental mode (HE_{11} mode) are excited in the SMF. Therefore, it can be drawn by computing the Poynting vector propagating along the z-direction of the FPS. Figures 8 and 9 show the Poynting vector propagating in the z-direction computed using the IFME. Figure 8 shows $\bar{S}^{(y)}(z)$ and $\bar{S}^{(x)}(z)$ of the step type, and Fig. 9 shows $\bar{S}^{(y)}(z)$ and $\bar{S}^{(x)}(z)$ of the graded type. From the shape of each Poynting vector, it can be confirmed

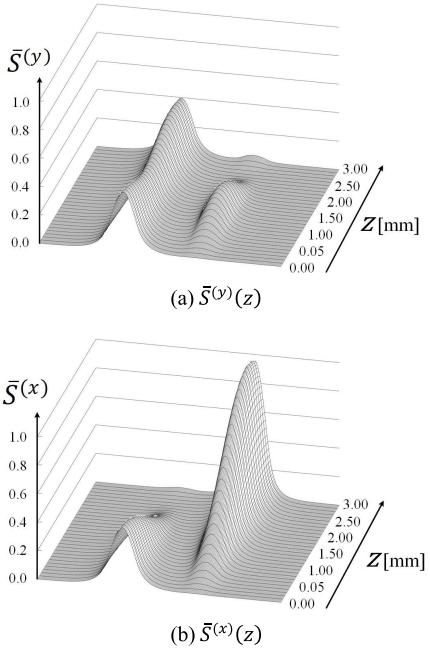

(a) $\bar{S}^{(y)}(z)$

(b) $\bar{S}^{(x)}(z)$

Fig. 8 Poynting vector propagating z-direction. (Step type)

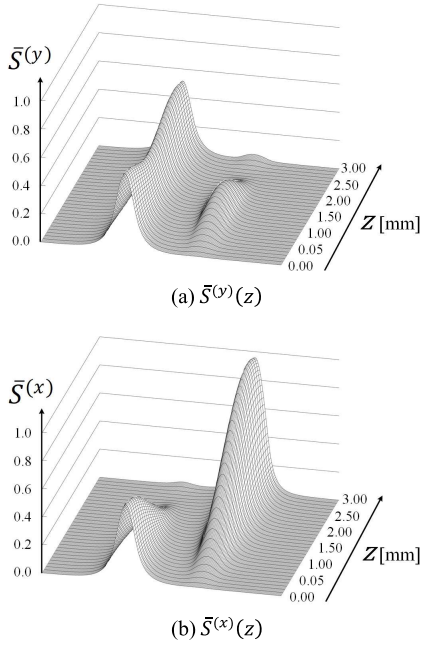

(a) $\bar{S}^{(y)}(z)$

(b) $\bar{S}^{(x)}(z)$

Fig. 9 Poynting vector propagating z-direction. (Graded type)

that both the step and graded types operate as FPS.

Figures 10 and 11 show the power transition characteristics of $P_i^{(x)}(z)$ and $P_i^{(y)}(z)$ ($i = 1, 2$). Figure 10 shows the results for the step type and Fig. 11 shows the results for the graded type. $P_i^{(y)}(z)$ and $P_i^{(x)}(z)$ are represented by solid and dashed lines, respectively, and the results of CMT and IFME are represented by black and blue lines, respectively. The following conclusions can be derived from Figs. 10 and 11:

(A1) Although the value of the power in the z-direction

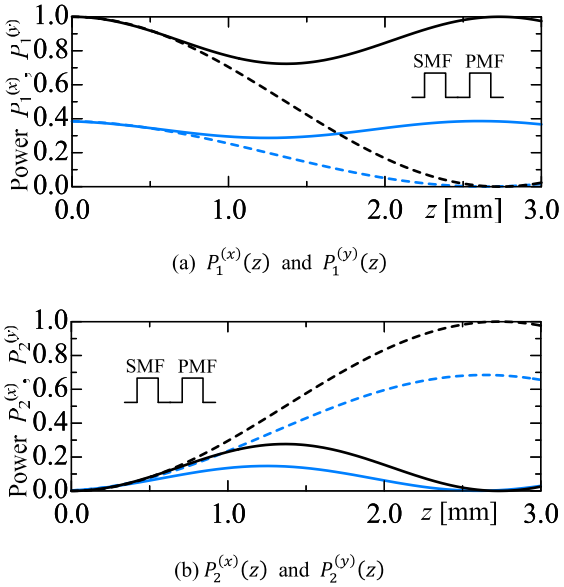

(a) $P_1^{(x)}(z)$ and $P_1^{(y)}(z)$

(b) $P_2^{(x)}(z)$ and $P_2^{(y)}(z)$

Fig. 10 Power transition characteristics along z direction. (Step type)

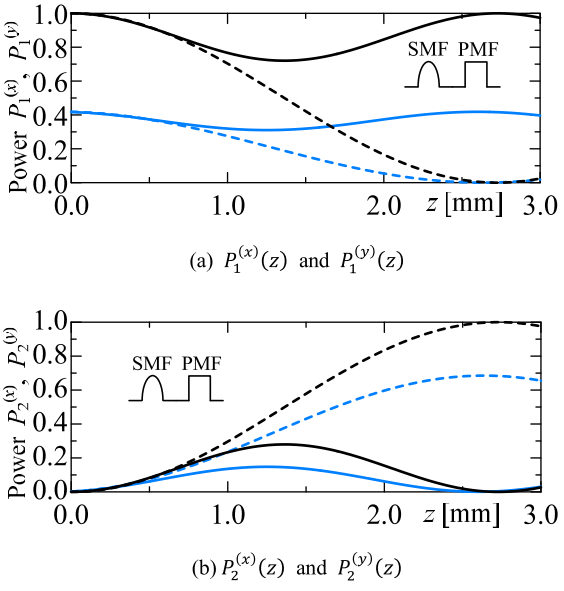

(a) $P_1^{(x)}(z)$ and $P_1^{(y)}(z)$

(b) $P_2^{(x)}(z)$ and $P_2^{(y)}(z)$

Fig. 11 Power transition characteristics along z direction. (Graded type)

differs between the CMT and IFME, the changes in the power transition characteristics are the same.

(A2) In the case of the step type, the device length L_y of the IFME is 2.603 mm. L_y of the CMT is 0.129 mm greater than that of the IFME.

(A3) In the case of the graded type, the device length L_y of the IFME is 2.602 mm. L_y of the CMT is 0.125 mm greater than that of the IFME.

Figure 12 shows the bandwidth BW against the extinction ratio R [8] of the step (solid lines) and graded (broken lines) types. The operation wavelength λ_{op} = 1550 nm is certainly included in BW. In Fig. 12, the vertical axis ΔBW_p ($p = s$ or g, s: step type, g: graded type) of right side is the

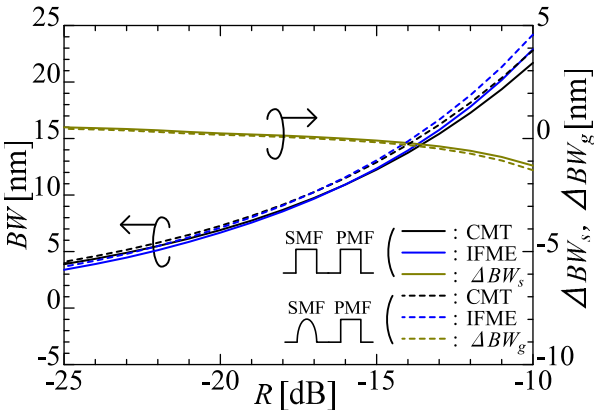

Fig. 12 Band characteristics.

value obtained by subtracting the extinction ratio of CMT from the extinction ratio of IFME. The results of the CMT, IFME, and ΔBW_p are indicated by black, blue, and olive lines, respectively. In the range of $15 \le |R| \le 20$ dB, which is an important reference value for the band of the FPS, it is found that the bandwidths of the CMT and IFME are almost the same and ΔBW_s becomes slightly smaller than ΔBW_g. In case of the graded type, the IFME bandwidth at $|R| = 15$ dB was 13.05 nm and $\Delta BW_g = 0.15$nm.

Figures 10–12 show that a slight difference in the device length and band characteristics exists between the CMT and IFME. This could be because at $z = 0$ in the power transition characteristics, $P_1^{(\gamma)}(z)$ starts at 1 and $P_2^{(\gamma)}(z)$ starts at 0 in the CMT, whereas in the IFME, a negligible power (approximately $P_1^{(\gamma)}(z)/160$ at step type and $P_1^{(\gamma)}(z)/180$ at graded type) is excited into Core 2. However, in this FPS, the CMT is sufficiently useful as a design method for weak coupling.

Figure 13 shows the deviation in the bandwidth characteristics when the excitation position of the HE_{11} mode is shifted from the center of the SMF. This is based on the assumption that when the SMF on the input side is bent, the electromagnetic field distribution is shifted from the center and is excited to the polarization splitter [31]. As shown in Fig. 13 (a), the excitation position is shifted by a distance $a_1/4$ from the center to three points: leftward, rightward, and upward (in consideration of symmetry). In the results of the band characteristics for the step type (Fig. 13 (b)) and the graded type (Fig. 13 (c)), no shift (center), leftward shift, rightward shift, and upward shift are denoted by black, green, blue, and red lines, respectively. The following conclusions can be drawn from Fig. 13:

(B1) For both the step type and graded type, the leftward shift and the rightward shifts of the excitation point slightly move the band characteristics to the right and left, respectively. These bandwidths remained almost unchanged for both the leftward and rightward shifts.

(B2) Among the band characteristics obtained from the three excitation points, the upward shift has the greatest influence, for which the minimum value of

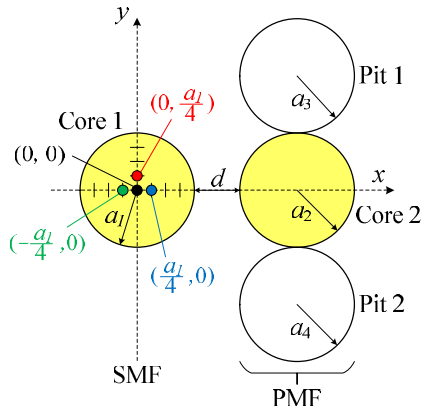

(a) Position exciting HE_{11} mode into SMF at z=0.

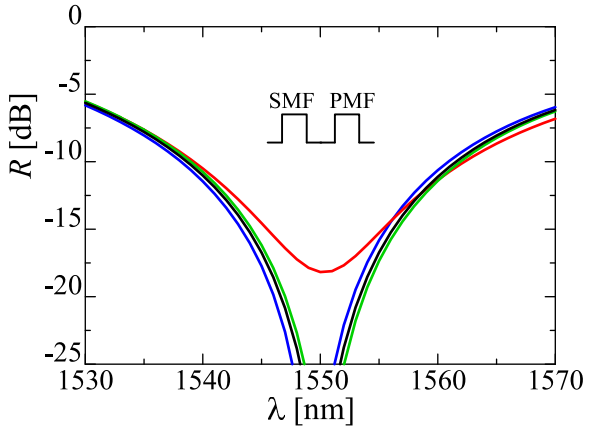

(b) Band characteristics. (Step type)

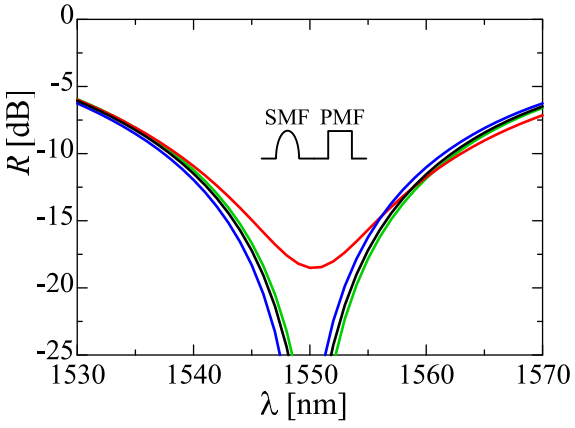

(c) Band characteristics. (Graded type)

Fig. 13 Bandwidth characteristics due to deviation of excitation position.

R for the step type and the graded type is −18.17 dB and −18.50 dB, respectively.

4. Conclusion

In this study, the proposed FPS was investigated using two methods for coupling analysis (CMT and IFME). The FPS propagation constant and electromagnetic field required for the coupling analysis were calculated using the PMM-DM, which is capable of high-precision analysis. The FPS consisted of an SMF and a PMF, and the cases with step type and graded type refractive index profiles of the core in the SMF were analyzed. In addition, the effect of the excitation point shift of the HE_{11} mode was investigated using IFME. The main results obtained from the analyses of the device length and band characteristics are as follows.

(C1) The device lengths obtained from CMT and IFME cause a slight difference of 0.129 mm for the step type and 0.125 mm for the graded type.

(C2) In the range of $15 \leq |R| \leq 20$ dB, which is an important reference value for the band of the FPS, it is found that the bandwidths of the CMT and IFME are almost the same and ΔBW_s becomes slightly smaller than ΔBW_g. In case of the graded type, the IFME bandwidth at $|R| = 15$ dB was 13.05 nm and $\Delta BW_g = 0.15$nm.

(C3) In this FPS, although our IFME can obtain more accurate results, the CMT is also sufficiently useful as a design method for the range of weak coupling.

(C4) Among the band characteristics obtained from the three excitation points, the upward shift has the greatest influence, for which the minimum value of R for the step type and the graded type is −18.17 dB and −18.50 dB, respectively, and R cannot be reduced beyond this value.

In future, we discuss the adaptation of CMT and IFME for actual fiber type coupling system devices and plan to continue developing devices with excellent properties while applicably determining availability and compatibility of two analysis methods.

References

[1] R.B. Dyott and J. Bello, "Polarisation-holding directional coupler made from elliptical cored fibre having a D section," Electron. Lett., vol.19, no.16, pp.601, Aug. 1983.

[2] M.S. Yataki, D.N. Payne, and M.P. Varnham, "All-fibre polarising beam splitter," Electron. Lett., vol.21, no.6, pp.249–251, March 1985.

[3] T. Bricheno and V. Baker, "All-fibre polarization splitter/combiner," Electron. Lett., vol.21, no.6, pp.251–252, March 1985.

[4] A.W. Snyder and A. Stevenson, "Polarisation splitters and birefringent couplers," Electron. Lett., vol.21, no.2, pp.75–77, Jan. 1985.

[5] A.W. Snyder, "Polarising beamsplitter from fused-taper couplers," Electron. Lett., vol.21, no.14, pp.623–625, July 1985.

[6] R. Stolen, A. Ashkin, J. Bowers, J. Dziedzic, and W. Pleibel, "Polarization-selective fiber directional coupler," J. Lightwave Technol., vol.3, no.5, pp.1125–1129, Oct. 1985.

[7] A.W. Snyder and A.J. Stevenson, "Polished-type couplers acting as polarizing beam splitters," Opt. Lett., vol.11, no.4, pp.254–256, April 1986.

[8] R. Hereth and G. Schiffner, "Broad-band optical directional couplers and polarization splitters," IEEE J.Lightwave Technol., vol.7, no.6, pp.925–930, June 1989.

[9] K. Kameda and T. Hosono, "Characteristics of polarization splitters constructed from a circular hollow pit outside the cores," Trans.

IEICE Japan, vol.J78-C-I, no.6, pp.273–281, June 1995. (Japanese edition)
[10] K. Kameda, S. Furukawa, and T. Hosono, "Characteristics of polar1zation splitter constructed from coupled two optical fibers," Trans. IEICE Japan, vol.J80-C-l, no.11, pp.491–500, Nov. 1997. (Japanese edition)
[11] A.W. Snyder, "Coupled-mode theory for optical fibers," Journal of the optical society of America., vol.62, no.11, pp.1267–1277, Nov. 1972.
[12] D. Marcuse, Light Transmission Optics, Bell Laboratories Series, New York, 1972.
[13] A.W. Snyder and J.D. Love, Optical Waveguide Theory, Chapman & Halls, London, 1983.
[14] A. Ankiewicz, A. Snyder, and X.-H. Zheng, "Coupling between parallel optical fiber cores–critical examination," J. Lightwave Technol., vol.4, no.9, pp.1317–1323, Sept. 1986.
[15] A.W. Snyder and A. Ankiewicz, "Fiber couplers-optimum solution for unequal cores," J. Lightwave Technol., vol.LT-6, no.3, pp.463–474, March 1988.
[16] T. Arakawa, K. Tanaka, K. Kameda, and S. Furukawa, "A design method of polarization splitters with circular cores and hollow pits," The Papers of Technical Meeting on Electromagnetic Theory, IEE Japan, The Papers of Technical Meeting on Electromagnetic Theory, EMT-18-114, pp.41–46, Nov. 2018. (Japanese edition)
[17] K. Tanaka, T. Arakawa, K. Kameda, and S. Furukawa, "An Analysis of Characteristics of a Polarization Splitter with Circular Cores and Hollow Pits," The 2019 IEICE general conference, C-1-9, March 2019. (Japanese edition)
[18] H. Matsumaru, M. Nagasaka, K. Kameda, and S. Furukawa, "An Analysis of Characteristics of a Polarization Splitter Composed of Circular Cores with Arbitrary Refractive Index Profiles and Hollow Pits," IEICE Technical Report EMT2020-40, pp.70–75, Nov. 2020. (Japanese edition)
[19] N. Kameyama, T. Hinata, and T. Hosono, "Propagation characteristics of optical fiber with two cores.," The IEICE general conference, C-1-17, Aug. 1988. (Japanese edition)
[20] S. Furukawa, K. Kameda, T. Hinata, and T. Hosono, "Coupling characteristics of three core optical fibers – An applicable range of coupled mode theory," The 1992 IEICE general conference, C-45, March 1992. (Japanese edition)
[21] K. Kameda, S. Furukawa, T. Hinata, and T. Hosono, "Coupling characteristics of optical fibers with two cores," IEE Japan, The Papers of Technical Meeting on Electromagnetic Theory, EMT-93-39ÅCpp.11–19ÅCMay, 1993. (Japanese edition)
[22] S. Tazawa, H. Matsumaru, T. Arakawa, K. Kameda, and S. Furukawa, "Coupling analysis of an optical waveguide with arbitrary arranged several inhomogeneous cores," IEICE Technical Report, EMT2019-84, pp.57–62, Nov. 2020. (Japanese edition)
[23] S. Tazawa, K. Kameda, and S. Furukawa, "Coupling characteristics of an optical waveguide with arbitrary arranged multiple inhomogeneous circular cores," IEICE Technical Report, EMT2020-39, pp.64–69, Jan. 2020. (Japanese edition)
[24] H. Matsumaru, S. Tazawa, T. Arakawa, K. Kameda, S. Furukawa, "An analysis of Optical Waveguides consisted of Circular Core with Arbitrarily Refractive Index Profiles by Point Matching Method," 2019 URSI-Japan Radio Science Meeting, BP-33, Tokyo, Japan, Sept. 2019.
[25] H. Matsumaru, T, Arakawa, S. Tazawa, K. Kameda, and S. Furukawa, "Characteristics analysis of waveguides coupled a few cores with arbitrary refractive index profile," IEICE Technical Report, EMT2019-48, pp.45–48, Oct. 2019. (Japanese edition)
[26] H. Matsumaru and S. Furukawa, "A Characteristic Analysis of a Single-Polarization Single-Mode Fiber with Multiple Circular Regions," IEICE Technical Report, EMT2020-49, pp.12–17, Jan. 2021. (Japanese edition)
[27] Y. Mochida, K. Shida, T. Arakawa, and S. Furukawa, "A Characteristic Analysis for a Single-Polarization Single-Mode Fiber Consisted of Circular Regions," IEICE Technical Report, EMT2022-115, pp.37–40, Nov. 2022. (Japanese edition)
[28] C. Vassallo, "Circular Fourier Analysis of Full Maxwell Equations for Arbitrarily Shaped Dielectric Waveguides-Application to Gain Factors of Semiconductor Laser Waveguides," J. Lightwave technol., vol.8, no.11, pp.1723–1729, Nov. 1990.
[29] H. Etzkorn and W.E. Heinlein, "Low-dispersion single-mode silica fibre with undoped core and three F-doped claddings," Electronics Letters, vol.20, no.10, pp.423–424, May 1984.
[30] M.J. Adams, An introduction to optical waveguide, John Wiley & Sons, New York, 1981.
[31] D. Marcuse, "Field deformation and loss caused by curvature of optical fibers," Journal of the Optical Society of America, vol.66, no.4, pp.311–320, April 1976.

Taiki Arakawa received the B.S. and M.S. degrees in electrical engineering from Nihon University, Tokyo, Japan, in 2020 and 2022, respectively. He is presently with Kandenko Co. Ltd, Tokyo, Japan and pursuing the Ph.D. degree in electrical engineering in Nihon University, Tokyo, Japan.

Kazuhiro Yamaguchi received the B.S. degree in electrical engineering from Nihon University, Tokyo, Japan in 2022. He is presently pursuing the M.S. degree in electrical engineering in Nihon University, Tokyo, Japan. His research interests are optical waveguide theory.

Kazunori Kameda received the B.S., M.S., and Ph.D. degrees in electrical engineering from Nihon University, Tokyo, Japan, in 1989, 1991, and 1998, respectively. He is presently a Professor with Sano Nihon University College, Tochigi, Japan. His research interests focus on optical waveguide theory.

Shinichi Furukawa received the B.S., M.S., and Ph.D. degrees in electrical engineering from Nihon University, Tokyo, Japan, in 1982, 1984, and 1988, respectively. He worked at Amano Co., Ltd., Kanagawa, Japan, from 1984 to 1989, Nihon University Junior College, Chiba, Japan, from 1989 to 1990, and Sano Nihon University College, Tochigi, Japan, from 1991 to 2011. He is presently a Professor with College of Science and Technology, Nihon University, Tokyo, Japan. His research interests focus on optical waveguide theory.